Equation of state, phase stability, and amorphization of SnI_4 at high pressure and temperature

Brent Grocholski*
Department of Earth, Atmospheric, and Planetary Sciences, Massachusetts Institute of Technology, 77 Massachusetts Avenue, Cambridge, Massachusetts 02130, USA

Sergio Speziale
Helmholtz Centre Potsdam, GFZ German Research Centre for Geosciences, Section 3.3, Telegrafenberg, D 228, D-14473 Potsdam, Germany

Raymond Jeanloz
Department of Earth and Planetary Science, University of California–Berkeley, 307 McCone Hall, Berkeley, California 94720-4767, USA
(Received 3 November 2009; revised manuscript received 20 January 2010; published 2 March 2010)

We have measured the pressure-induced amorphization of tin iodide (SnI_4) as a function of temperature and found a small (<1 GPa) increase in the initiation pressure of the transition from 293 to 523 K. We have also determined the *P-V* equation of state while the material undergoes the amorphization, including multiple compressions of a single sample, using a diamond-anvil cell and x-ray diffraction. Apparent stiffening upon multiple compression of the sample can be explained by either an increase in nonhydrostaticity during loading or, possibly, changes in the initial crystal structure upon decompression recrystallization. Contrary to previous interpretations of the amorphization being a two-stage process, with SnI_4 converting to a second (unidentified) crystalline phase before the loss of Bragg intensities, the present experiments show that it is also possible to amorphize SnI_4 without the appearance of the second crystalline phase. While the new diffraction peaks appear upon the first compression of a sample, subsequent compressions of the same sample do not show these new peaks; instead, long-range ordering of the original cubic crystal structure is lost.

DOI: 10.1103/PhysRevB.81.094101 PACS number(s): 62.50.−p, 81.40.Vw, 61.05.cp, 64.70.P−

I. INTRODUCTION

Tin iodide (SnI_4) is a van der Waals-bonded molecular solid with a cubic structure at atmospheric pressure. The crystal structure at room pressure and temperature, determined by Dickenson[1] and further refined by Meller and Fankuchen,[2] can be described as containing SnI_4 tetrahedra arranged in a face-centered-cubic lattice.[3] Under compression at room temperature at around 15 GPa, SnI_4 undergoes reversible solid-state amorphization that was first recognized using x-ray diffraction[4] and Raman scattering.[5] This transition was initially thought to involve only the original cubic crystal phase (CPI) but this interpretation has been challenged by the observation of a second crystal phase (CPII) at about 7.5 GPa.[6] While several theories have been proposed to account for the loss of Bragg intensity with pressure,[7,8] the idea of pseudomelting[7,9] has been invoked specifically to account for the amorphization of tin iodide with pressure.

Amorphization of tin iodide is accompanied by a large increase in electrical conductivity, first noticed by Riggleman and Drickamer.[10] Metallization, which is achieved by 15 GPa, requires this weakly bonded material to generate enough orbital overlap for electron delocalization in order to account for the electrical conductivity increase with pressure. Mössbauer spectroscopy using ^{119}Sn and ^{129}I suggests that the material may be polymerizing, forming $-(SnI_4)_x-$ chains of random length that account for both the amorphous character of the sample and the increase in electrical conductivity.[3] This interpretation is supported by additional Mössbauer and conductivity measurements in the diamond cell.[11] However, the appearance of CPII happens to occur at the same pressure as the increase in conductivity and this correspondence suggests that metallization may be due to CPII (Ref. 6) rather than amorphization of the sample.

We have conducted a set of experiments to determine the change in amorphization pressure with temperature and measured the equation of state at room temperature for pristine and multiply recompressed samples. We have found that, in certain cases, the appearance of CPII is not necessary in order to amorphize the sample. In addition, we have crystallized a new phase of tin iodide at low pressure (2.7 GPa) through sudden decompression of the sample at temperatures above 573 K.

II. EXPERIMENTAL METHOD

Nine samples of SnI_4 (Alfa Aesar, 99.998% purity) were loaded in rhenium gaskets and compressed in a diamond-anvil cell to roughly 20 GPa in order to fully amorphize each sample. We used a membrane cell and diamonds with 350 μm culets. The sample chamber was roughly 100 μm in diameter and 15–25 μm thick. Pressure was measured using the equation of state of gold[12] with either a gold flake (samples 1–5) or a ~60:40 mixture of SnI_4 to gold powder (samples 6–9). The gold was used as an internal pressure and intensity standard. Powder x-ray diffraction patterns were taken at approximately 1 GPa pressure intervals, using a 25 keV x-ray beam of ~20 μm diameter at the Advanced Light Source Beamline 12.2.2. Data were collected for ~100–200 s with a MAR-345 image plate (Fig. 1).

Heating was performed using a ring heater positioned inside the cell body. The diamond-anvil cell was placed in a container flushed with inert gas (argon with 5% hydrogen).

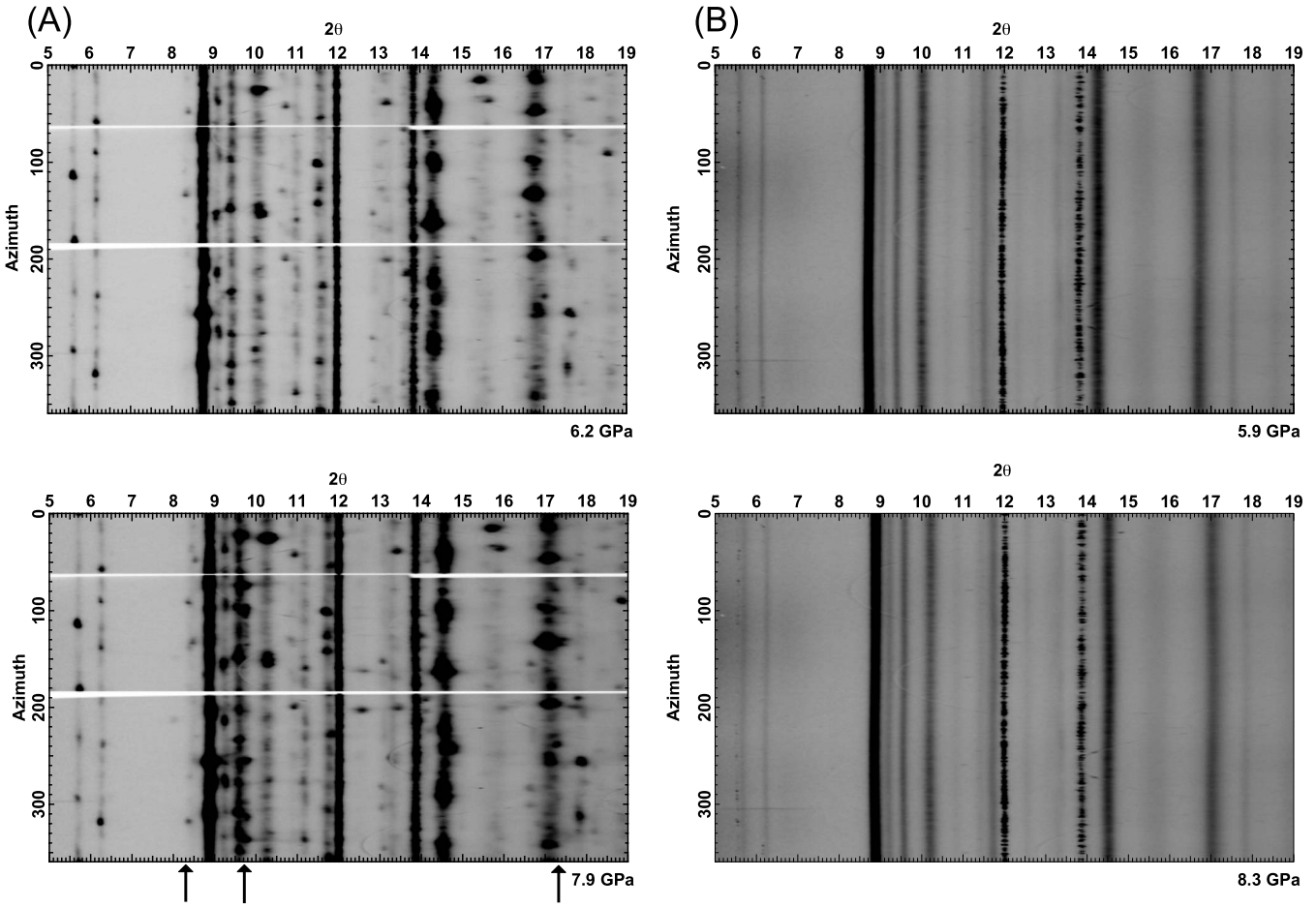

FIG. 1. X-ray diffraction intensity as a function of scattering angle 2θ (in degrees) and azimuth for SnI_4 at comparable pressures for two different samples: first compression of a sample at 293 K (sample 6) on the left and fourth compression at 373 K (sample 5.4) on the right. Three new diffraction lines appear as spots on the left (arrows). Spottiness is absent on the right and the diffraction lines are smooth due to a broad distribution of crystal grain orientations relative to the x-ray beam. No new diffraction features appear in this sample above 7 GPa. In addition, the 311 reflection to the left of the highest intensity 222 line ($2\theta \sim 9$) is also absent.

The container design allowed the x-ray beam to reach the sample, but made optical access impossible, preventing the use of ruby fluorescence for pressure calibration. The temperature was measured using a thermocouple that was placed within 1 mm of the diamond tips. The temperature inside the ring heater had been previously calibrated but no further attempts were made to measure the temperature *in situ*. While the temperature measurement has $1°-2°$ precision, the absolute accuracy of the temperature measured in experiments is only $\sim 25°$. This is in part due to insufficient and irregular thermal insulation of the ring heater from the diamond backing plates.

Sample 1 was cryogenically loaded with an argon pressure medium but this was found to be unnecessary because tin iodide is a soft material ($K_0 \sim 11$ GPa) and does not appear to benefit from the presence of a quasihydrostatic pressure transmitting medium. Therefore, subsequent samples (2–9) were loaded without argon. A separate sample (sample 10) was loaded at room temperature and compressed a total of two times to assess the nonhydrostatic pressure gradient using the ruby fluorescence technique.[13] The pressure variation was found to be at most 0.5 GPa at 20 GPa, for both the first and second compressions of the sample. This is consistent with previously reported measurements of pressure variations across SnI_4 samples loaded inside gasketed diamond cells.[4,14] Most of the samples in this experiment were taken to high temperature, which also reduces pressure gradients due to nonhydrostaticity (Table I).

III. RESULTS

A. Equation of state

We compressed nine different samples of tin iodide a total of 13 times. Figures 1(A) and 2(A) show an example, with the patterns illustrating the appearance of the new phase CPII at roughly 7.5 GPa as noted by Hamaya *et al.*[6] Most of the intensity of the new peaks comes from individual spots that are easiest to see in Fig. 1(A) in the pattern collected at 7.9 GPa. Most of the samples that we compressed showed the same behavior between 6 and 8 GPa. Figure 1(B) shows diffraction patterns from a sample that had been pressure amorphized and recrystallized by decompression three times before recompression at 373 K (sample 5.4). The patterns are

TABLE I. Summary of all experimental data runs. The second column gives the range of pressure over which the Birch-Murganhan equation of state was fit. Parameters (K_{0T}, K'_{0T}) are given for both third and second-order fits for room-temperature samples. High-temperature samples were not fit due to poor constraint of V_0. Amorphous transition pressures in general are estimates based on the intensity decrease in the 440 reflection with pressure and the general resolvability of the diffraction pattern as a whole. The transition pressure for sample 5.2–5.5 were determined by fitting the decrease in intensity of the 440 reflection and taking the 50% value using Eq. (1) (Fig. 4).

Sample No.	P	T (K)	K_{0T}	K'_{0T}	K^*_{0T}	P_t	Comments
1	2.4–15.0	293	12.2(5)	3.5(2)	10.6(1)	~12–15	Argon loaded
2	4.0–14.7	348				~13	
3	2.4–19.5	398				~15–19	CPII absent
4	7.7–21.7	448				~17–19	Much higher P_t than other samples
5.1	0.2–16.9	523				~17–19	Multiple compressions, last 4 not showing any evidence of CPII;
5.2	2.1–17.6	488					
5.3	0.1–17.0	448				~14.2	
5.4	5.6–17.3	373				~15.4	
5.5	0–17.8	293	13.5(4)	4.2(3)	14.2(1)	~14.5	V_0=12.12(2)
6	0.6–16.7	293	8.9(4)	5.4(2)	10.6(1)	~14–15	
7	3.2–13.7	573				>13.7	Gasket failure CPII appears ~5.3 GPa
8	3.2–16.6	>573				>14–16	Gasket failure, new phase appears upon decompression to 2.3 GPa. No CPII with second compression
9	0–3.0	598					Loses 311 and 331 diffraction lines upon decompression from 3 GPa
1+6	0–16.7	293–573	10.4(3)	4.1(1)	10.6(1)		V_0=12.261(1)

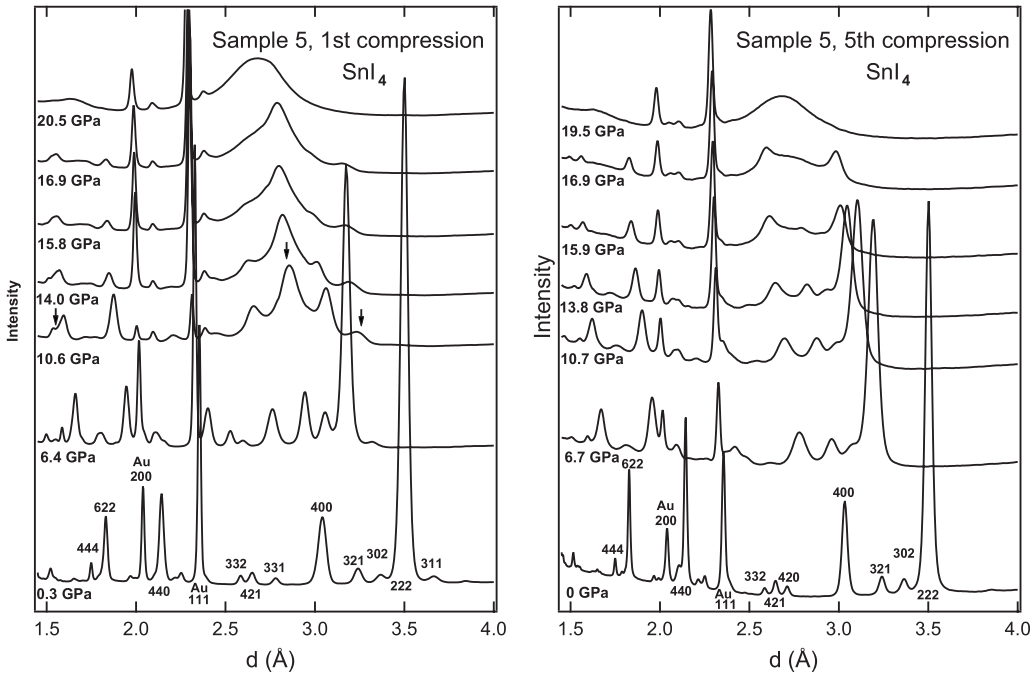

FIG. 2. Integrated x-ray diffraction for sample 5 at various pressures. The patterns on the left are for the first compression (at 523 K) while the patterns on the right are from the fifth compression of the same sample after four decompression crystallizations from the amorphous state. Arrows indicate the appearance of CPII in the diffraction pattern. The lack of CPII in the right pattern makes it easier to extract the positions of diffraction lines: especially the 622 and 444 reflections. The sample amorphizes in both cases at roughly the same pressure.

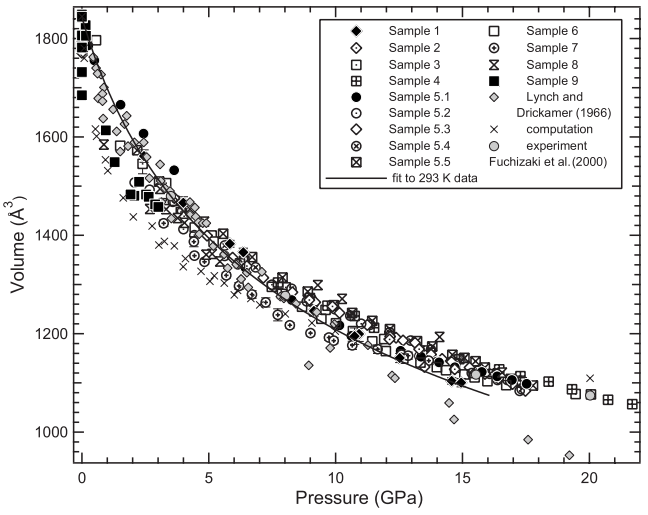

FIG. 3. Pressure-volume plot for all data. The data in gray are from previous studies. The volumes were calculated using 2 to 12 reflections of the cubic crystal structure. The large deviation in Lynch and Drickamer (Ref. 16) at high pressures may be due to a misidentification of the amorphous humps as the 222 and 622 reflections. All our pressures were determined using gold as an internal standard.

much smoother than those of Fig. 1(A) due to smaller and more randomly oriented grains that form during recrystallization, along with no indication of CPII formation. All diffraction patterns collected from sample 5 (runs 5.2–5.5) have a similar smoothness and absence of the CPII diffraction lines.

The integrated x-ray diffraction patterns are shown in Fig. 2 from a sample collected at 523 K (sample 5.1) upon its initial compression and the same sample at 293 K (sample 5.5) during its fifth compression. The 0 GPa diffraction patterns from the recrystallized samples (5.2–5.5) are similar, but not identical, to the pattern of the initial sample: the 311 and 331 diffraction lines are missing and the 420 reflection appears in these recrystallized samples. The lattice parameter of the unit cell also appears to be ~1.1% smaller [a_0 =12.12(2) Å] than our room-pressure value of 12.261(1) Å, after compressing the sample four times. The change in intensity of lattice reflections is perplexing, as 420 is not a forbidden reflection but has zero intensity as long as the SnI_4 tetrahedra are not distorted. Tetrahedral distortion can decrease the 311, 331 intensities to zero, but the 420 reflection should be accompanied by the 411 reflection—which is not observed in this sample. This behavior is not limited to sample 5, as the same reflections are lost in sample 9 upon catastrophic decompression from 3 GPa to room pressure at 598 K without any amorphization. Sample 8 has the 420 reflection but also contains the 311, 331, and 411—indicating that tetrahedral distortion is possible.

Our measurements of unit-cell volumes are consistent with values reported by Fuchizaki *et al.*[15] and up to 15 GPa with the data of Lynch and Drickamer[16] (Fig. 3). Above 15 GPa, the low volumes from Lynch and Drickamer are probably due to misidentification of the amorphous humps as the peak positions of the 222 and 622 reflections. Background increases due to pressurization and amorphization combined with apparent peak broadening from the appearance of CPII make different *hkl* lattice reflections become unresolved at different pressures. Volumes are calculated from 8 to 12 reflections at low pressure and 2 to 4 reflections at high pressure. Most of the volumes in Fig. 3 fall within a few percent of the average volume for any given pressure. The scatter is due in part to the high compressibility of the material—errors in pressures can lead to large relative errors in volume. Many of the deviations appear to be systematic and potentially dependent on the initial conditions of the sample or the specific pressure distribution in the sample chamber.

A third-order isothermal Eulerian finite-strain (Birch-Murnaghan) equation of state[12] was used to fit the volumes collected from samples 1 and 6 at room pressure, with a V_0 of 1843.2 Å^3 and the recompressed sample 5.5 was fit with a resulting V_0 of 1780.4 Å^3. The values for the bulk modulus and pressure derivative are K_{0T}=10.6(1) GPa and K'_{0T} =4.1(1) (subscripts zero and T indicate zero pressure and isothermal conditions, respectively). Fitting with a fixed K'_{0T}=4 (corresponding to a second-order Birch equation of state) gives a bulk modulus of 10.6(1) GPa. The recompressed sample volumes increasingly deviate from the measured first-compression volumes with each compression. The divergence occurs within the range at which the CPII lines appear in the reference data and may reflect lack of stress (pressure) relaxation across our sample and between the various phases present (including the pressure calibrant). The result after four compressions is an increase in bulk modulus at room temperature to K_{0T}=13.6(1) GPa with K'_{0T}=4.2(3) or K_{0T}=14.2(1) GPa with K'_{0T}=4. At pressures above 15 GPa all of the isothermal compression curves collapse back on each other when all of the samples are mostly amorphous.

B. Pressure-induced amorphization

Figure 2 shows a comparison between amorphization with and without the appearance of CPII in the integrated diffraction pattern. The diffraction patterns in Fig. 2(A) are similar to those previously published,[4,6] with the location of the CPII diffraction lines shown as arrows on the 10.6 GPa trace. The sample eventually amorphizes at 13–15 GPa, although determining the point at which this happens is difficult due to the appearance of the CPII diffraction lines. The traces shown in Fig. 2(B) demonstrate the sample can become amorphous without the appearance of a second (CPII) crystal phase. In this case, it becomes much easier to quantify the amorphization pressure. We quantify how the intensity of the 440 diffraction line of SnI_4 changes with pressure, relative to the 111, 220, or 311 gold lines, because its intensity correlates well with the overall change in diffraction pattern (see Fig. 2) and it is the last peak to lose intensity upon amorphization.

The results are fitted to Eq. (1),

$$\frac{I_{sample}}{I_{calibrant}} = 0.5 \times \left\{ 1 - \tanh \frac{P - P_t}{w_t} \right\}. \quad (1)$$

The amorphous transition pressure (P_t) is the point at which the normalized relative intensity is at 50% and w_t is a mea-

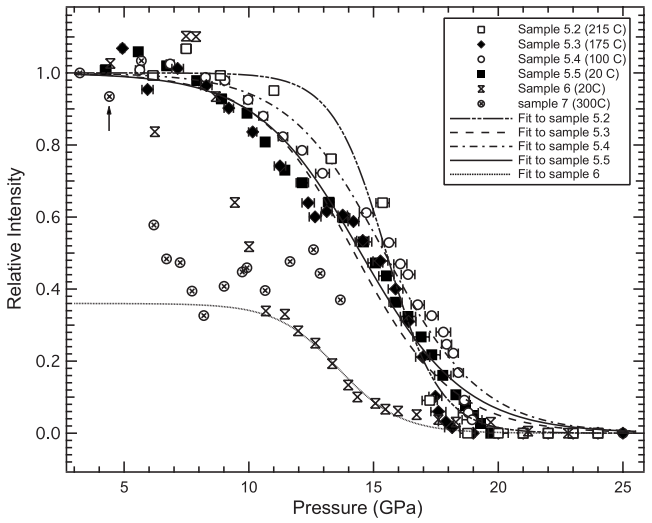

FIG. 4. Normalized intensity as a function of pressure for the (440) reflection. The data have been fit using Eq. (1) and the parameters for the fits are in Table II. The normalized intensities from samples 6 and 7 are plotted for comparison—there appears to be an initial decrease in the relative intensity due to the appearance of new diffraction lines in the sample. This makes it difficult to define the initial intensity and therefore quantify the amorphous transition pressure. We fit the high-pressure (>10 GPa) data for sample 6 by rescaling the zero-pressure relative intensity. Sample 7 does not appear to have undergone an amorphization and upon sudden decompression from ~13 to ~4 GPa (arrow), recovers a reasonable relative intensity of ~1.0.

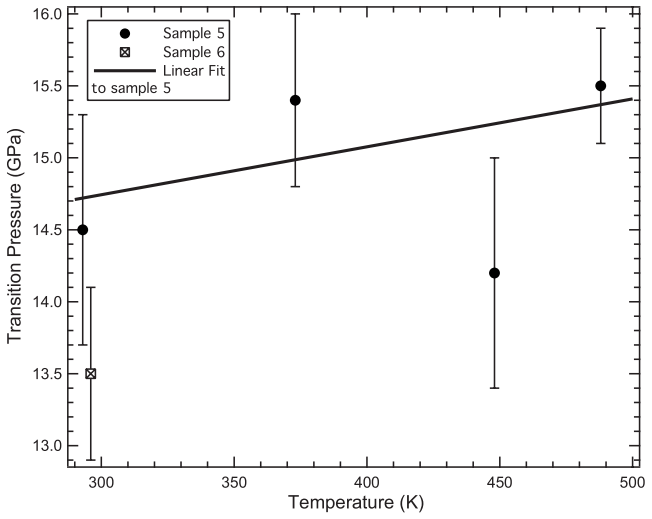

FIG. 5. Transition pressure as a function of temperature as determined by fits to the data in Fig. 4. Sample 6 was collected at 293 K but has been shifted to 296 K to make it easier to see the error on the measurement. The data from sample 5 were fit using linear regression. Error bars were determined by taking the difference between the transition pressure and the pressure at which the normalized intensity was 40% or 60%.

sure of the width of the amorphization (Fig. 4). In order to minimize the effect of pressure-induced amplitude reduction, the 100% value is taken as the average of the sample to calibrant ratios of data points ranging from 4 to 6 GPa. Samples 6 and 7 are plotted to show the difference between how the intensity of the 440 line falls off as a function of pressure when the new diffraction lines (CPII) appear in the sample. Sample 6 was fit using a renormalized form of Eq. (1), as well, although due to the appearance of (CPII) we need to take the 100% intensity value at 11 GPa instead of lower pressure. The transition pressure as a function of temperature (or compression) is given in Table II. The error on each value of P_t was determined by differencing the pressure at which the intensity was 40% and 60% of the original intensity. These data are plotted in Fig. 5 and a least-squares fit to the transition pressures gives a slope of 3.3(±4.1) MPa/K and an intercept of 13.7(±1.8) GPa. In all cases, these are amorphization pressures obtained by increasing the pressure of the sample.

TABLE II. Parameters from fitting sample 5 in Fig. 4 with Eq. (1).

Compression	P_t (GPa)	w_t (GPa)
2	15.5(0.4)	2.2(0.4)
3	14.2(0.8)	3.9(0.3)
4	15.4(0.6)	3.9(0.3)
5	14.5(0.8)	4.2(0.2)

Amorphization pressures were estimated qualitatively for the different sample loadings that have the CPII phase and are listed as a range in Table I. In general, P_t for different samples appears to be load dependent, ranging from a low of ~13 GPa for sample 2 to a high of 17–19 GPa for sample 4. Our results are consistent with Hamaya *et al.*'s[6] findings that document a large hysteresis in the amorphization transition, with the reverse transformation (amorphous→crystalline) occurring below 1.8 GPa.

IV. DISCUSSION

Over the course of 13 sample compressions and roughly 300 diffraction patterns, the most consistent observation was the loss of diffraction intensity that documented the appearance of an amorphous material. These high-pressure amorphous solids recrystallized upon pressure release, generating crystals with smaller grain size than the initial sample. The amorphization takes place regardless of temperature or the appearance of CPII. The repeatable amorphization combined with the tendency to measure uniform volumes when the sample is mainly amorphous indicates that much of the scatter in the volume data and irreproducibility in the number of crystal phases in the sample is dependent on the specifics of the sample stress environment (and perhaps history). The weak intermolecular forces in tin iodide may make it sensitive to even small deviatoric stresses, which can change the amorphization pressure of crystals.[17] At pressures above 15 GPa, all samples appear to behave about the same, apparently due to a more uniform stress environment from sample to sample.

There are several possible reasons for the differences in the amorphization pressure between different samples and sample loadings. If we treat the temperature dependence of the transition pressure as that of a first-order transition we can define a Clayperon slope as Eq. (2),

$$\frac{dP_t}{dT} = \frac{\Delta S}{\Delta V}, \tag{2}$$

where the change in volume should be negative. The data collected for sample 5 and shown in Fig. 5 has a slightly positive slope of 3.3(±4.1) MPa/K that implies little or no change in entropy between CPI and the amorphous state. This is consistent with the interpretation of the pressure-induced amorphization of calcium hydroxide.[18] The variation in amorphization pressures among our samples may also be due to subtle differences in the deviatoric stresses between samples. Catalli *et al.*[17] have found the pressure-induced amorphization of $Ca(OH)_2$ is likely facilitated by nonhydrostatic (deviatoric) stress and they do not observe this transition in a quasihydrostatic pressure medium (argon). Although the nonhydrostatic stresses in our system appear to be relatively low (<0.5 GPa at 20 GPa), tin iodide may be extremely sensitive to even small deviatoric stresses that change the amorphization pressure by up to several gigapascals.[19]

The pressure-volume curve in Fig. 3 shows that, although we have a fairly consistent general trend, significant deviations appear that are not easy to explain without considering nonhydrostatic effects. In the case of sample 5, it appears that the recrystallization does not produce quite the same material as we started with. After each decompression cycle the sample appears to have smaller unit-cell volumes and, possibly, slightly distorted tetrahedra. This results in less compressible crystals (i.e., an increase in the bulk modulus).

These types of deviations are likely due to the sample environment (i.e., deviatoric stress, grain size, and internal strains) as the uniformity of the measured volumes above 15 GPa is due to all samples being primarily amorphous and presumably reflect a similar sample environment between different loadings. Figure 6 shows an example where shear (via gasket blowout) generates a new (presumably metastable) phase of tin iodide. This brings up the possibility that CPII is a shear-induced phase as well that can coexist with CPI until the sample becomes disordered and it converts to an amorphous solid, either directly or via back-conversion to CPI as is seen in Fig. 6.

Regardless of the nature of the CPI-CPII phase boundary, there is no need for the sample to go through the CPII phase for amorphization. The production of the amorphous phase from two different crystal structures seems to undermine the pseudomelting hypothesis as suggested by Fuchizaki *et al.*[20] The two materials that have been cited as examples of pseudomelting are water-ice[9] and quartz,[21] and both are thought to have the negative dT_m/dP melting slopes necessary for the melt curve to return to low temperature: a requirement for explaining room-temperature amorphization according to this model. That the melting slope of SnI_4 is positive, according to molecular-dynamics simulations[15,20,22,23] and direct measurement,[23] seems to eliminate this hypothesis. Moreover, pseudomelting may not explain high-pressure amorphization, in general, as many systems produce an amorphous state appearing like a highly disordered crystal[24] or exhibiting a memory of the crystal phase from which it came.[25] Assuming that both paths to amorphization (CPI→CPII→amorphous or CPI →amorphous) are possible, this would support the idea that mechanical destabilization due to polyhedral disordering causes loss of long-range order, such as proposed by Tse and Klug[26] for SiO_2. Such disordering may well be consistent with the idea of SnI_4 chains being formed, as well, resulting in the observed increase in electrical conductivity.[3]

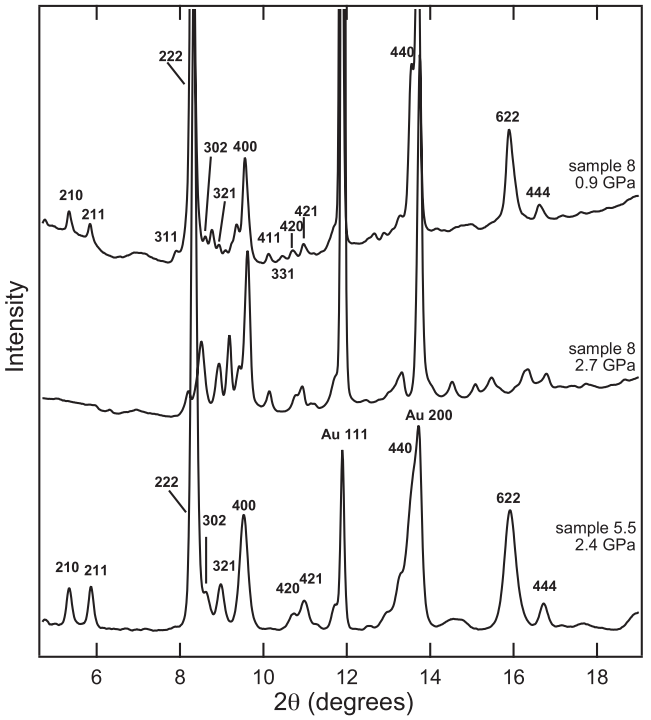

FIG. 6. Comparison of data collected at similar pressures (~2.5 GPa) and at 0.9 GPa (sample 8) as an example of a mixed-phase diffraction pattern. Sample 8 at 2.7 GPa is missing all of the major diffraction lines. The major lines are all present in the mixed-phase pattern along with a number of reflections (i.e., 411 and 420) that have zero intensity for the SnI_4 structure provided the tetrahedra are regular.

V. CONCLUSION

We have conducted a set of experiments to determine the change in amorphization pressure with temperature and have measured the equation of state of SnI_4 at room temperature. We have found that the appearance of a second crystal phase is not necessary in order to amorphize the sample. More generally, our results seem inconsistent with the pseudomelting hypothesis, instead favoring other mechanisms of amorphization. Since both CPI and CPII amorphize eventually, it seems likely that there is at least one additional thermodynamically stable (crystalline) phase at high pressures. The possibility also remains that the glass formed is the stable phase, especially in light of a zero or positive Clayperon

slope. Finally, we have also observed a new, shear-induced metastable phase of tin iodide, obtained by sudden partial decompression of the sample from high pressure.

ACKNOWLEDGMENTS

The authors would like to thank Simon Clark, Martin Kunz, Sander Caldwell, and A. E. Gleason for experimental assistance. We would like to thank Dave Walker for the construction and calibration of the heating apparatus, and the anonymous reviewers for helpful comments. We acknowledge the use of the facilities of beamline 12.2.2. at the Advanced Light Source, Lawrence Berkeley National Laboratory. The Advance Light Source is supported by the Director, Office of Science, Office of Basic Energy Sciences, Materials Sciences Division, of the U.S. Department of Energy under Contract No. DE-AC03-76SF00098 at Lawrence Berkeley National Laboratory.

*b.grocholski@gmail.com

[1] R. Dickenson, J. Am. Chem. Soc. **45**, 958 (1923).
[2] F. Meller and I. Fankuchen, Acta Crystallogr. **8**, 343 (1955).
[3] M. Pasternak and R. D. Taylor, Phys. Rev. B **37**, 8130 (1988).
[4] Y. Fujii, M. Kowaka, and A. Onodera, J. Phys. C **18**, 789 (1985).
[5] S. Sugai, J. Phys. C **18**, 799 (1985).
[6] N. Hamaya, K. Sato, K. Usui-Watanabe, K. Fuchizaki, Y. Fujii, and Y. Ohishi, Phys. Rev. Lett. **79**, 4597 (1997).
[7] S. Sharma and S. Sikka, Prog. Mater. Sci. **40**, 1 (1996).
[8] A. Pereira, C. A. Perottoni, and J. da Jornada, J. Raman Spectrosc. **34**, 578 (2003).
[9] O. Mishima, L. Calvert, and E. Whalley, Nature (London) **310**, 393 (1984).
[10] B. Riggleman and H. Drickamer, J. Chem. Phys. **38**, 2721 (1963).
[11] A. L. Chen, P. Y. Yu, and M. P. Pasternak, Phys. Rev. B **44**, 2883 (1991).
[12] D. Heinz and R. Jeanloz, J. Appl. Phys. **55**, 885 (1984).
[13] H. Mao, J. Xu, and P. Bell, J. Geophys. Res., [Solid Earth Planets] **91**, 4673 (1986).
[14] A. Ohmura, N. Hamaya, K. Sato, C. Ogawa, M. Isshiki, and Y. Ohishi, J. Phys.: Condens. Matter **14**, 10553 (2002).
[15] K. Fuchizaki, S. Sugiyama, and Y. Fujii, J. Chem. Phys. **112**, 10379 (2000).
[16] R. Lynch and H. Drickamer, J. Chem. Phys. **45**, 1020 (1966).
[17] K. Catalli, S. Shim, and V. Prakapenka, Geophys. Res. Lett. **35**, L05312 (2008).
[18] W. Caldwell, Ph.D. thesis, University of California–Berkeley, 2000.
[19] K. J. Kingma, C. Meade, R. Hemley, H. Mao, and D. Veblen, Science **259**, 666 (1993).
[20] K. Fuchizaki, S. Sugiyama, and Y. Fujii, J. Phys. Soc. Jpn. **70**, 1321 (2001).
[21] R. Hemley, A. Jephcoat, H. Mao, L. Ming, and M. Manghnani, Nature (London) **334**, 52 (1988).
[22] K. Fuchizaki and K. Nagai, Solid State Commun. **132**, 305 (2004).
[23] K. Fuchizaki, Y. Fujii, A. Ohishi, N. Hamaya, Y. Katayama, and T. Okada, J. Chem. Phys. **120**, 11196 (2004).
[24] M. Kruger and C. Meade, Phys. Rev. B **55**, 1 (1997).
[25] M. Kruger and R. Jeanloz, Science **249**, 647 (1990).
[26] J. S. Tse and D. D. Klug, Phys. Rev. Lett. **67**, 3559 (1991).